RESEARCH ARTICLE SUMMARY

NEURODEVELOPMENT

The coding and long noncoding single-cell atlas of the developing human fetal striatum

Vittoria Dickinson Bocchi, Paola Conforti, Elena Vezzoli, Dario Besusso, Claudio Cappadona, Tiziana Lischetti, Maura Galimberti, Valeria Ranzani, Raoul J. P. Bonnal, Marco De Simone, Grazisa Rossetti, Xiaoling He, Kenji Kamimoto, Ira Espuny-Camacho, Andrea Faedo, Federica Gervasoni, Romina Vuono, Samantha A. Morris, Jian Chen, Dan Felsenfeld, Giulio Pavesi, Roger A. Barker, Massimiliano Pagani*, Elena Cattaneo*

INTRODUCTION: The striatum modulates distinct characteristics of human social behavior and is an area affected in many neurological diseases. We created a comprehensive single-cell atlas of this area during early human fetal development, considering both protein-coding transcripts and long intergenic noncoding RNAs (lincRNAs).

RATIONALE: Understanding of the molecular mechanisms that define human striatal development has been limited by the scarcity of relevant fetal tissue and the use of only a limited panel of protein-coding genes in most gene identification studies. We created a cell-specific molecular atlas of the lateral ganglionic eminence (LGE), the striatal primordium. Our first goal was to develop a catalog of de novo identified lincRNAs of this area using bulk RNA sequencing. This catalog should help to clarify the specific characteristics of human development because lincRNAs exhibit accelerated evolution, are highly cell-specific, and are required for brain development. Our second goal was to understand how the medium spiny neurons (MSNs), the principal cell types in the striatum, differentiate and diversify, and which genes act as master regulators of fate determination. MSNs diversify into D1 and D2 types, so named for their expression of one of the two variants of the human dopamine receptor (D1 and D2). We used single-cell RNA sequencing to infer the developmental landscape of MSNs and to define and validate fate markers.

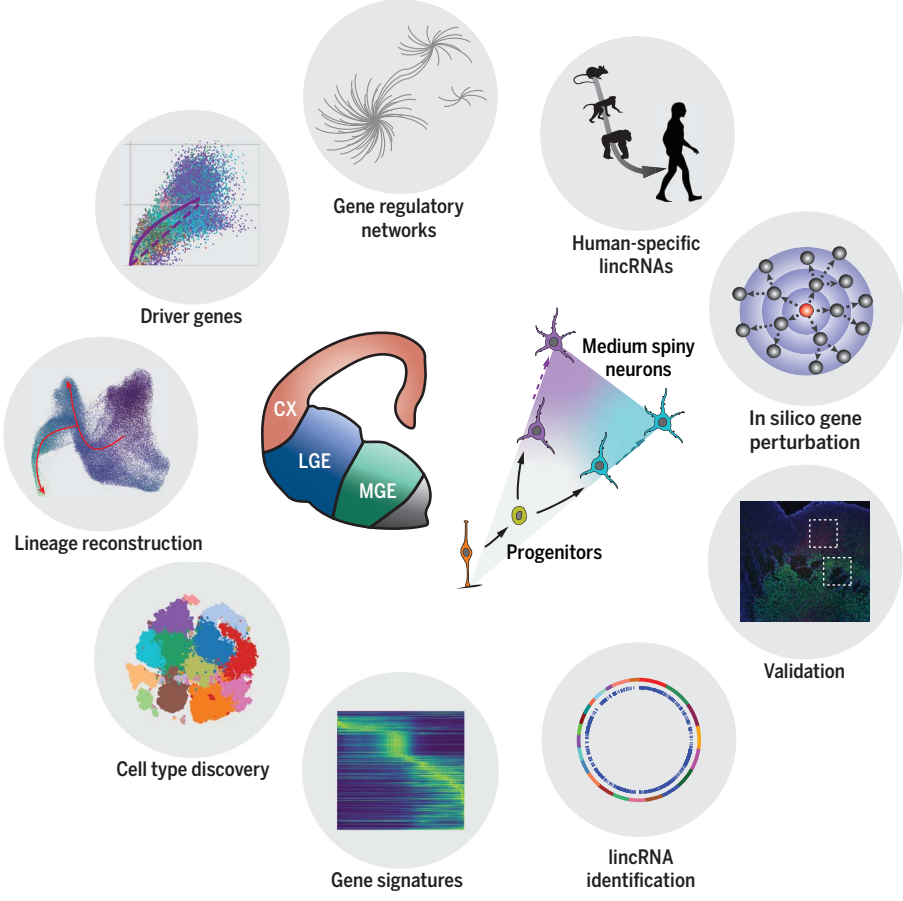

The molecular blueprint of striatal development. Combined bulk and single-cell RNA sequencing of the human fetal striatum reveals cell states together with their key coding and lincRNA fate determinants, and defines the developmental hierarchies underlying lineage commitment in medium spiny neurons. CX, neocortex; LGE, lateral ganglionic eminence; MGE, medial ganglionic eminence.

ILLUSTRATION: TIZIANA LISCHETTI

RESULTS: Bulk RNA sequencing enabled the annotation of 1116 novel lincRNAs of different areas of the human developing telencephalon, and we found that these lincRNAs are less conserved among species than those previously identified in the adult brain. Bulk measurements enabled us to pinpoint the distinctive signature of the striatum relative to surrounding areas, and we determined that huntingtin (HTT) is a specific upstream regulator of this region. We then profiled 96,789 single cells of the LGE, based on both coding RNAs and the newly identified lincRNAs. This enabled us to uncover the transcriptional profiles of 15 different cell states that included lincRNAs that were gained throughout evolution. We found that a common progenitor generates both D1- and D2-MSNs and that this progenitor is distinct from the progenitor of interneurons. We also discovered a postmitotic precursor cell state for both D1- and D2-MSNs, which falls within a continuum of key fate determinants. Finally, we identified a panel of gene regulatory networks that define D1- and D2-MSNs, and we showed that in silico knockout of the transcription factors governing these networks could cause the arrest of both MSN lineages, blockage of a specific MSN class, or switching between MSN fates.

CONCLUSION: Our findings reveal the differentiation hierarchies that govern human striatal development. We anticipate that the set of transcription factors and lincRNAs identified in this study will be leveraged to recreate MSN differentiation in vitro and that these cells can then be used for cell replacement therapies in Huntington's disease (HD). Furthermore, we expect that this atlas will guide investigations of the developmental components related to HD. Finally, we foresee that our lincRNA catalog will contribute to understanding the additional layer of fine-tuning mechanisms present in the human striatum but not in other species. ■

The list of author affiliations is available in the full article online.
*Corresponding author. Email: elena.cattaneo@unimi.it (E.C.); massimiliano.pagani@unimi.it (M.P.)
Cite this article as V. D. Bocchi *et al.*, *Science* **372**, eabf5759 (2021). DOI: 10.1126/science.abf5759

READ THE FULL ARTICLE AT
https://doi.org/10.1126/science.abf5759

RESEARCH ARTICLE

NEURODEVELOPMENT

The coding and long noncoding single-cell atlas of the developing human fetal striatum

Vittoria Dickinson Bocchi[1,2], Paola Conforti[1,2], Elena Vezzoli[1,2]†, Dario Besusso[1,2], Claudio Cappadona[1,2]‡, Tiziana Lischetti[1,2], Maura Galimberti[1,2], Valeria Ranzani[2], Raoul J. P. Bonnal[2]§, Marco De Simone[2]¶, Grazisa Rossetti[2]§, Xiaoling He[3], Kenji Kamimoto[4,5,6], Ira Espuny-Camacho[1,2]#, Andrea Faedo[1,2]**, Federica Gervasoni[2,7]§, Romina Vuono[3]††, Samantha A. Morris[4,5,6], Jian Chen[8], Dan Felsenfeld[8], Giulio Pavesi[1], Roger A. Barker[3], Massimiliano Pagani[2,7]§*, Elena Cattaneo[1,2]*

Deciphering how the human striatum develops is necessary for understanding the diseases that affect this region. To decode the transcriptional modules that regulate this structure during development, we compiled a catalog of 1116 long intergenic noncoding RNAs (lincRNAs) identified de novo and then profiled 96,789 single cells from the early human fetal striatum. We found that D1 and D2 medium spiny neurons (D1- and D2-MSNs) arise from a common progenitor and that lineage commitment is established during the postmitotic transition, across a pre-MSN phase that exhibits a continuous spectrum of fate determinants. We then uncovered cell type–specific gene regulatory networks that we validated through in silico perturbation. Finally, we identified human-specific lincRNAs that contribute to the phylogenetic divergence of this structure in humans. This work delineates the cellular hierarchies governing MSN lineage commitment.

The striatum, a subcortical structure made up of the caudate nucleus and putamen, is important in motor control and learning, procedural behavior, cognition, and emotional and motivational responses. Many of these functions are associated with uniquely human abilities including the development of speech and language (*1*). In adults, the striatum is primarily composed of medium spiny neurons (MSNs) carrying either D1-type or D2-type dopamine receptors interspersed with aspiny interneurons (*2*). This organization does not appear to vary among species (*3*). However, this apparent homogeneity in cellular composition masks functional complexity of human-specific striatal circuits.

[1]Dipartimento di Bioscienze, Università degli Studi di Milano, Milan, Italy. [2]INGM, Istituto Nazionale Genetica Molecolare, Milan, Italy. [3]WT-MRC Cambridge Stem Cell Institute and Department of Clinical Neuroscience, University of Cambridge, Cambridge, UK. [4]Department of Developmental Biology, Washington University School of Medicine, St. Louis, MO 63110, USA. [5]Department of Genetics, Washington University School of Medicine, St. Louis, MO 63110, USA. [6]Center of Regenerative Medicine, Washington University School of Medicine, St. Louis, MO 63110, USA. [7]Dipartimento di Biotecnologie Mediche e Medicina Traslazionale, Università degli Studi di Milano, Milan, Italy. [8]CHDI Management/CHDI Foundation, New York, NY, USA. †Present address: Department of Biomedical Sciences for Health, Università degli Studi di Milano, 20133 Milan, Italy. ‡Present address: Department of Biomedical Sciences, Humanitas University, Pieve Emanuele 20090 Milan, Italy. §Present address: IFOM-FIRC Institute of Molecular Oncology, Milan, Italy. ¶Present address: Department of Radiation Oncology, Cedars-Sinai Medical Center, Los Angeles, CA, USA. #Present address: Université de Liège, GIGA Stem Cells, Quartier hôpital 15, B-4000 Liège, Belgium. **Present address: Axxam, OpenZone, 20091 Bresso, Milan, Italy. ††Present address: Medway School of Pharmacy, University of Kent, Chatham, Kent, UK.
*Corresponding author. Email: elena.cattaneo@unimi.it (E.C.); massimiliano.pagani@unimi.it (M.P.)

During development, MSNs are derived from progenitors in the lateral ganglionic eminence (LGE) of the telencephalon (*4*). Most studies of this area have concentrated on rodent models and the coding signature of limited cell types. Long noncoding RNAs (lncRNAs) have a higher tissue specificity than mRNAs (*5*) and a diversity that correlates more closely with brain complexity than protein-coding genes (*6*). LncRNAs may, therefore, better discriminate cell states during striatal development in humans.

In this study, we first conducted bulk RNA-seq to identify novel long intergenic noncoding RNAs (lincRNAs) expressed in the developing human LGE that we then leveraged to define the spatial coding and noncoding map for this area that discriminates it from the surrounding neocortex (CX) and medial ganglionic eminence (MGE). We then performed single-cell RNA-seq (scRNA-seq) to characterize cell diversity in the LGE, identify LGE-specific coding and noncoding cell states, define cell type–specific gene regulatory networks and decipher pivotal bifurcation points in the formation of human MSNs. Finally, we performed in silico perturbations by knocking out and overexpressing key transcription factors (TFs) of the MSN lineage, together with immunohistochemistry and fluorescence in situ hybridization (FISH) analysis to validate our findings.

lincRNA discovery and scRNA-seq profiling of the human LGE

To identify unannotated putative lincRNAs expressed during human striatal development, we dissected the CX, LGE, and MGE from human embryos between 7 and 20 post-conceptional weeks (pcw), with at least two or three biological replicates for each developmental stage (table S1). We then profiled by RNA-seq the transcriptome of each area (Fig. 1A) and set up a computational pipeline (fig. S1A) to create a corresponding catalog of lincRNAs (fig. S1, B to E). Because our bulk RNA-seq protocol was unstranded, and because genic lncRNAs are difficult to correctly predict without strand information discriminating them from overlapping genes, we decided to include only a reliable set of intergenic lncRNAs (lincRNAs). To better understand the relationship between lincRNAs identified in other tissues and our newly identified lincRNAs, we integrated two catalogs derived from different human tissues and cell types (*7*, *8*), plus a lincRNA catalog of the developing human CX (*9*), into this study.

We detected 1116 novel lincRNA loci (Fig. 1B and table S2), among which the highest number was found in the developing LGE and the lowest in the CX (fig. S1F), probably because of the greater extent of data available from the CX. We found that lincRNAs had an average of 2.27 exons; this was also the case for all lincRNA catalogs integrated into this study, with the exception of the FANTOM catalog, which used CAGE-seq instead of classic RNA-seq and showed fewer exons (fig. S1G). For each sampled pcw, we then defined a signature of protein-coding genes and lincRNAs that were uniquely expressed in either the LGE, the CX, or the MGE (Fig. 1C, fig. S2A, and table S3). Gene Ontology (GO) analysis in the LGE between 7 and 11 pcw revealed an enrichment for terms related to neural differentiation and to forebrain and subpallium development (fig. S2B and table S4), whereas at 20 pcw this changed to regulation of synaptic plasticity and neurotransmitter secretion, reflecting the more mature state of the 20-pcw striatum (fig. S2C and table S4).

Pathway enrichment analysis (IPA, Ingenuity Systems) revealed huntingtin (HTT) as the most significant upstream regulator ($P < 0.001$) of the LGE at all time points considered (Fig. 1D, fig. S2D, and table S5). This suggests that HTT may have an important role in human striatal development.

To explore how these protein-coding genes and lincRNAs define specific cell states during development of the human striatum, we surveyed 96,789 high-quality single cells from the LGE between 7 and 11 pcw (Fig. 1A and table S1). We were able to discriminate 15 clusters and their transcriptional signatures (Fig. 1E and table S6) that were then classified according to canonical markers (Fig. 1F). Biological replicates were well distributed in each detected cluster (fig. S3A), and all time points considered between 7 and 11 pcw covered the identified clusters (fig. S3, B and C), indicating that during this stage of early development the same cell types are present. Both D1- and D2-MSN subtypes were

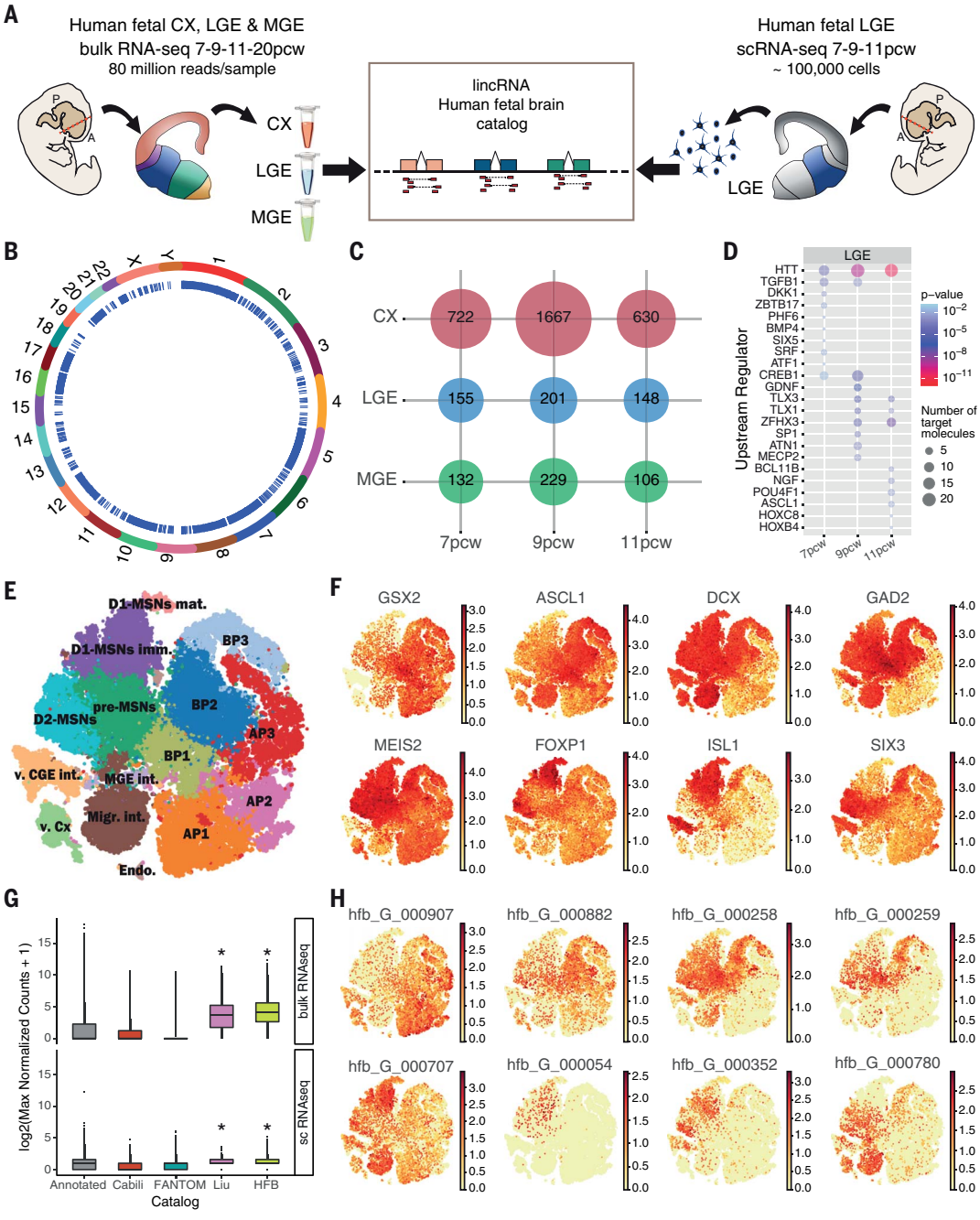

Fig. 1. The coding and noncoding transcriptional landscape of the developing human striatum. (**A**) Schematic representation of the experimental design. CX, neocortex; LGE, lateral ganglionic eminence; MGE, medial ganglionic eminence; pcw, post-conceptional weeks; A, anterior; P, posterior. (**B**) Circular plot showing the genomic location of 1116 novel lincRNAs. Outer ring, chromosomes; inner ring, loci of newly identified lincRNAs. (**C**) Bubble matrix showing the number of uniquely expressed protein-coding genes and lincRNAs per area and per pcw from bulk RNA-seq data. (**D**) Upstream regulators of the bulk LGE-specific signature between 7 and 11 pcw. (**E**) t-SNE (t-distributed stochastic neighbor embedding) plot of 96,789 single cells from the LGE between 7 and 11 pcw, color-coded by cell type. AP, apical progenitors; BP, basal progenitors; pre-MSNs, precursor medium spiny neurons; D1-MSNs imm., immature D1 medium spiny neurons; D1-MSNs mat., mature D1 medium spiny neurons; D2-MSNs, D2 medium spiny neurons; MGE int., MGE interneurons; Migr. int., migrating interneurons; v.CGE int., ventral caudal ganglionic eminence interneurons; v.Cx, ventral neocortical neurons; Endo., endothelial cells. (**F**) Gene expression levels of markers for early progenitors (*GSX2*), intermediate progenitors (*ASCL1*), neurons (*DCX*), GABAergic neurons (*GAD2*), LGE-lineage cells (*MEIS2*), general MSNs (*FOXP1*), D1-MSNs (*ISL1*), and D2-MSNs (*SIX3*). (**G**) Boxplot showing distribution of maximal normalized expression of lincRNAs from different catalogs in bulk and single-cell data. *$P < 2 \times 10^{-16}$ (pairwise comparisons: Liu (lincRNA catalog of the developing CX) versus FANTOM (lincRNA catalog of different adult tissues and cell types), Cabili (lincRNA catalog of different adult tissues and cell types), and annotated lincRNAs; HFB (human fetal brain; catalog of lincRNAs identified de novo in this study) versus FANTOM, Cabili, and annotated lincRNAs; Wilcoxon test with Bonferroni correction). Boxplots show the first, second, and third quartiles. Lines summarize values within 1.5 times the first and third interquartile ranges. Points beyond the whiskers are outliers. (**H**) Gene expression levels of highly specific lincRNAs identified de novo in this study.

present in all time points considered (fig. S3C) and were characterized by known markers such as *ISL1* in D1-MSNs and *SIX3* in D2-MSNs (Fig. 1F and fig. S4, A to C).

GO analysis revealed that apical progenitors (APs) are associated with terms such as cell adhesion and glial cell differentiation, mirroring the proliferating nature of this cell type. Basal progenitors (BPs) express genes related to mRNA splicing, RNA binding, and forebrain development, which suggests that a posttranscriptional control network coordinates and primes these cells for their final cell division and fate acquisition. Genes identified in the pre-MSN phase are enriched in GO terms linked to nervous system development and axon guidance, whereas D1- and D2-MSNs show a more mature gene signature linked to synapse organization and chemical synaptic transmission (fig. S4D and table S7).

Marginally contaminating populations of cells included *NKX2.1*-, *LHX6*-, and *LHX8*-expressing MGE interneurons, migrating interneurons, ventral neocortical cells, ventral caudal ganglionic eminence (CGE) cells, and endothelial cells (fig. S5, A to C). By subclustering the migrating interneurons, we were able to observe dorsal LGE (dLGE) interneurons expressing *SP8* and *COUP-TFII* (*NR2F2*) together with *PAX6*; we also observed MGE migrating interneurons

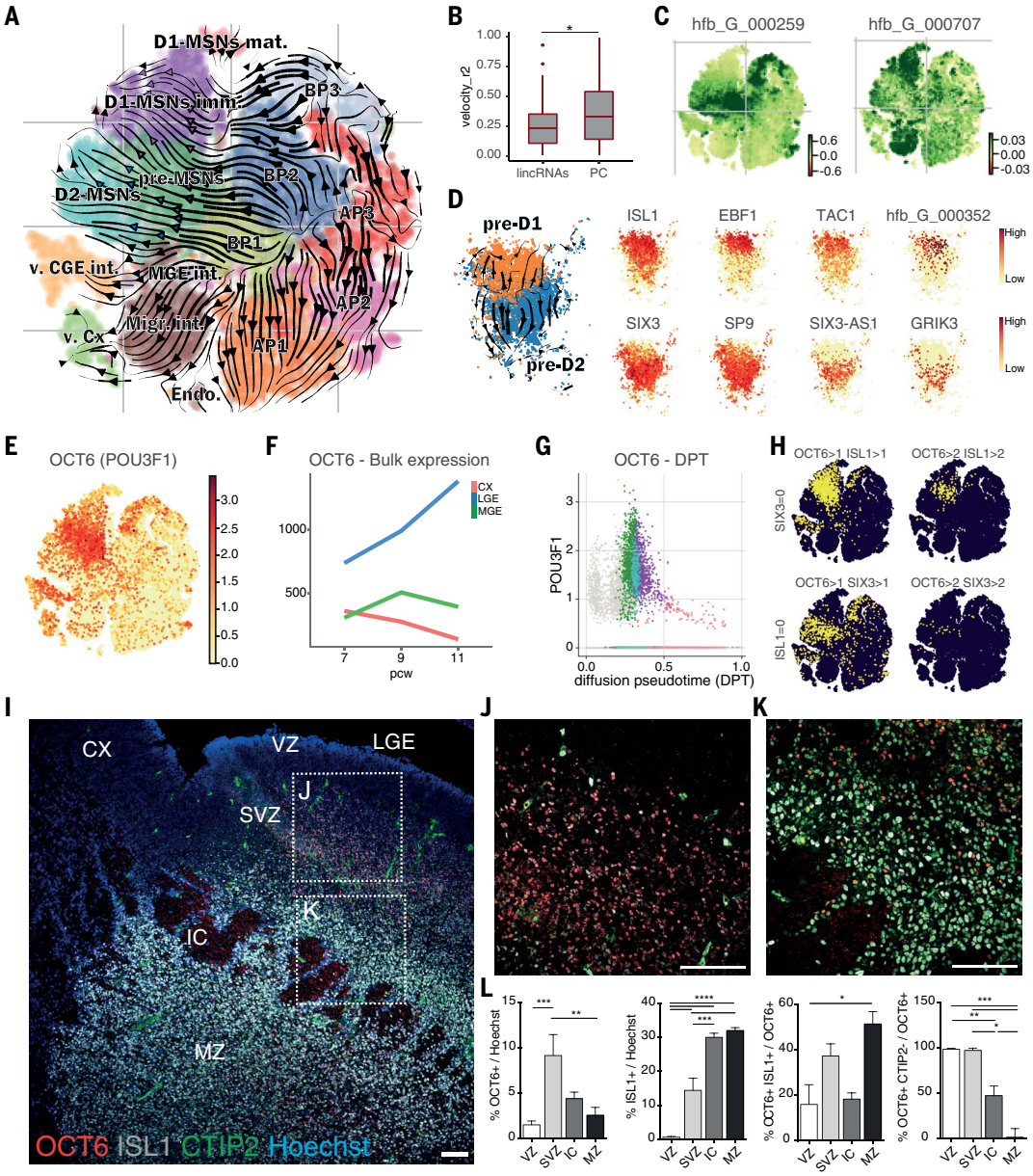

Fig. 2. Maturation and differentiation trajectory of MSNs. (**A**) Velocity estimates projected onto a two-dimensional t-SNE plot of the LGE dataset. Arrowheads in the pre-MSN cluster are colored according to commitment to either the D1 (purple) or D2 (cyan) MSN fate. (**B**) Boxplot showing splicing kinetics of lincRNAs and protein-coding genes. *P < 0.05 (Wilcoxon test with Bonferroni correction). (**C**) t-SNE plot showing velocities of each gene. Positive velocities (dark green) indicate that a gene is up-regulated, which occurs for cells that show higher abundance of unspliced mRNA for that gene than expected. (**D**) Subclusters within the pre-MSN cluster and the velocity vector fields, together with expression levels of canonical D1-MSN (top row) and D2-MSN (bottom row) markers. (**E** to **G**) Single-cell (E) and bulk (F) expression levels, together with single-cell expression levels (cells are colored according to Louvain cluster) plotted against pseudotime (G), of the pre-MSN specific marker *OCT6* (*POU3F1*). (**H**) t-SNE plot showing cells coexpressing *OCT6*/*ISL1* and *OCT6*/*SIX3* with different thresholds of gene expression (coexpressing cells are shown in yellow). (**I**) OCT6, ISL1, and CTIP2 staining of a telencephalic coronal hemisection at 9 pcw. IC, internal capsule. Scale bar, 100 μm. (**J** and **K**) Magnification (40×) of the SVZ and IC sections marked in (I). (**L**) Automatic quantification of the percentage of cells positive for OCT6, ISL1, and CTIP2 with the NIS software on confocal images at 40× magnification. N = 3 to 6 fields for each zone: VZ, SVZ, IC, and MZ from two or three coronal slices of one fetus; two or three z stacks of each field are pre-mediated. Statistics were performed with Prism: *P < 0.05, **P < 0.01, ***P < 0.001, ****P < 0.0001 (one-way analysis of variance, Bonferroni posttest).

expressing *NXK2.1* and *LHX6* that were presumably passing through the subventricular zone (SVZ) of the LGE at this developmental stage (because the same population did not express *LHX8*) (fig. S5, C and D). As expected, *ERBB4* was found in both types of migrating interneurons (fig. S5D). The findings that these two populations cluster together despite their different sites of origin and that subclustering was required to reveal their diversity suggest that their interneuron migratory class signature is stronger than their lineage of origin signature. We did not observe any markers of oligodendrocytes, astrocytes, or microglia, indicating that these cells appear later in normal human striatal development, and found no evidence of corridor cells that have probably migrated to the globus pallidus by 7 pcw in humans.

As previously reported (*7*), in our study bulk expression levels of lincRNAs are lower than those of protein-coding genes, and our single-cell data also show differential expression for these two biotypes (fig. S5E). However, when comparing the different catalogs, we observed that lincRNAs identified in the developing human CX (*9*) and those identified in this study (HFB) displayed higher transcript levels, both in bulk and single-cell data, relative to lincRNAs identified in different adult tissues (Fig. 1G). This suggests that these lincRNAs are associated with the development of the human telencephalon. Overall, lincRNAs are more specific than protein-coding genes both in bulk and single-cell measurements (fig. S5F). We found that these lincRNAs characterize different cell states of the LGE lineage; for example, the lincRNA *hfb_G_000907* is associated with APs, whereas *hfb_G_000258* characterizes pre-MSNs and D2-MSNs (Fig. 1H).

MSN differentiation passes through a pre-MSN cell state

To infer how fate decisions occur, we defined the cell trajectories that give rise to MSNs

using velocyto (*10*, *11*). The velocity field map (Fig. 2A) reflects the dynamics of MSN differentiation as these cells transition from APs to D1- and D2-MSNs, passing through a pre-MSN phase. This model shows that in the pre-MSN phase, there is already a separation between the D1 and D2 states (Fig. 2A). We found that lincRNAs display reduced splicing kinetics relative to protein-coding genes (Fig. 2B), reflecting their inefficient splicing (*12*). However, within the putative driver genes (table S8), we identified a number of lincRNAs that may guide MSN differentiation. These include *hfb_G_000259*, which shows pronounced velocities in BPs, pre-MSNs, and D2-MSNs, and *hfb_G_000707*, which contributes to the D1-MSN transition (Fig. 2C).

Overall, our data suggest that the same progenitors give rise to both D1- and D2-MSNs. Subclustering the AP and BP groups confirmed the absence of lineage commitment at these stages (fig. S6, A and B). This was further proved by calculating the connectivity between each cluster of the LGE lineage by means of partition-based graph abstraction (PAGA), which showed that progenitors are highly interconnected and converge to give rise to D1- and D2-MSNs through the pre-MSN phase (fig. S6C). To explore the potential temporal relationships between cell states in the LGE lineage, we used a measure of graph distance (diffusion pseudotime, DPT) (fig. S6, D and E). We observed that cell states and DPT recapitulate known temporal dynamics of neural maturation, with mitotic APs of the ventricular zone (VZ) having the lowest DPT score and mitotic BPs of the SVZ having an intermediate DPT score (fig. S6E). These findings suggest that the latter cells represent a more mature progenitor state, as reflected by the expression of *HES6*, which is found in cells committing to neural differentiation.

Pre-MSNs together with D1- and D2-MSNs were classified as postmitotic (fig. S6F) and showed the highest DPT score, which peaked in cells classified as mature D1-MSNs (fig. S6E). This cell population was the only one to express the more mature neuronal cytoskeleton marker neurofilament-M (*NEFM*) (fig. S6G), and most cells of this cluster are found at the most advanced pcw analyzed (fig. S3C). This temporal signature was confirmed using FISH (fig. S6H). Finally, at the cluster level, we found that splicing kinetics and differentiation accelerates substantially after cell cycle exit (especially in pre-MSNs and D2 neurons), maintaining pace during D2 production but slowing down during D1 production (fig. S6I). This finding is consistent with a model in which immature differentiating cells (D2-MSNs) are less transcriptionally stable and reveal greater splicing dynamics than terminally differentiated cells (D1-MSNs) (*13*). Overall, these findings suggest that both MSN subtypes are present at this early stage of development but that D1-MSNs mature and reach equilibrium at a faster rate than D2-MSNs.

We then focused on pre-MSNs because this cell state escaped previous identification. Subclustering of pre-MSNs revealed that these cells exhibit either a D1- or D2-MSN blueprint with enrichment of cell-specific markers of each subtype (Fig. 2D). Although subclustering revealed two discrete cell states, markers such as *SIX3*, *SP9*, and *ISL1* showed a gradient of opposing expression, with both markers found in both subclusters at different expression levels. We therefore tested different thresholds of *SIX3* and *ISL1* coexpression in the entire LGE lineage to test how the transcripts behaved throughout differentiation. We found that high levels of *SIX3* and low levels of *ISL1* are present in the D2-MSN lineage at the pre-MSN stage, and that coexpression is lost at terminal D2-MSN fates (fig. S7A). The opposite trend was seen for high *ISL1* and low *SIX3* in the D1 MSN lineage (fig. S7A). High levels of both transcripts were instead found in a very small percentage of cells (~7%), and this was also reflected at the protein level (fig. S4, B and C). This suggests that the pre-MSN phase spans a transcriptional continuum rather than being a discrete cell state.

We then identified *OCT6* (*POU3F1*), a member of the POU-III subfamily, as a specific marker of this pre-MSN cell state (Fig. 2E), as well as being LGE-specific (Fig. 2F) and exhibiting transient expression (Fig. 2G). When looking at its expression at the pre-MSN stage, we also found that this gene is more enriched in pre-D1 MSNs and appears to follow an expression gradient (fig. S7B). Examining coexpression levels of this transcript with candidate D1- and D2-MSN markers, we observed that low levels of *OCT6-ISL1* characterize the D1 lineage, whereas high levels define the pre-D1 state (Fig. 2H). Low levels of *OCT6-SIX3* were also found in D2-MSNs; however, very few positive cells were found with high expression of both markers (Fig. 2H). To confirm these findings, we performed systematic immunohistochemistry analysis of these markers at 9 pcw. We observed specific OCT6 staining in the SVZ of the LGE (Fig. 2, I to K), with none in the CX, MGE, and CGE (fig. S7C). We also found that OCT6-positive cells are postmitotic neurons, as only 2% are double-positive for the BP marker ASCL1 (fig. S7, D to G) and more than 80% of OCT6 cells do not express the proliferative marker Ki67 in the SVZ (fig. S7, H and I). Forty percent of OCT6 cells were positive for ISL1, and they were all negative for CTIP2, a marker of mature MSNs, showing that *OCT6* is a key gene of pre–D1-MSNs in the SVZ (Fig. 2, J to L). For pre-D2 MSNs, we found ~10% of OCT6 and SIX3–coexpressing cells in the SVZ (fig. S8, A to D). This suggests that the low OCT6 expression level characterizing this cell state translates into only a few cells detectable by immunohistochemistry. This low-to-high gradient is also observed with immunohistochemistry, where SIX3 cells were enriched dorsally and faded moving ventrally, whereas OCT6 showed a reverse ventral-to-dorsal enrichment (fig. S8A). These patterns of OCT6-ISL1 and OCT6-SIX3 coexpression in the SVZ were also confirmed at 11 pcw (fig. S8, E to H). To confirm the pre-D2 state, we looked at how ASCL1, SIX3, and CTIP2 behave in the SVZ (fig. S8I). We found that most of the SIX3-expressing cells in the SVZ lack expression of both ASCL1 and CTIP2 (fig. S8, J to L), confirming the presence of the pre-D2 state in the SVZ.

Our findings support a model in which D1- and D2-MSNs derive from a common progenitor; cells become postmitotic as they pass through a primed precursor phase that exhibits heterogeneity in the expression of key MSN regulators, and specific subtypes of MSNs are gradually established. If this model is correct, fate determination in MSNs does not occur as an instantaneous shift in cell fate, but rather is a smooth and continuous process that falls within two gradients of expression.

Gene regulatory networks of the MSN lineage

The human LGE domain has been the most elusive area of the basal ganglia to characterize. To bridge this gap, we applied SCENIC (*14*) to our scRNA-seq data and reconstructed the gene regulatory networks and combinatorial codes of TFs that define the different cell states in this domain (Fig. 3A and table S9). Overall, gene regulatory network analysis revealed that distinct regulons classify different axes of MSN development, with D1- and D2-MSNs sharing most of the active TFs (Fig. 3B). We found a number of TFs that were not previously associated with LGE development. These include OTX1 for APs, VAX1 for BPs, POU2F2 for both types of MSNs, NANOG in D2-MSNs, and FOXO1 for D1-MSNs.

We then used SCENIC coexpression networks to infer potential relationships between our de novo identified lincRNAs and our cell type–specific TFs (fig. S9A and table S10), because it has been shown that lincRNA loci contain many conserved TF binding sites (*12*), hence their relationship may be functionally relevant. We found that *hfb_G_000907*, a specific lincRNA of APs, is strongly linked to *SOX* genes, and that *hfg_G_000296*, another lincRNA specific for APs, shows a high connection with a PDZ-LIM domain family protein called PDLIM5. The BP lincRNA *hfb_G_00882* shows a correlation with *RARA*, an important mediator of retinoid signaling. For MSNs, we found common lincRNAs between D1- and D2-MSN subtypes that are in the same network with universal MSN signatures such as *ZNF467* and *POU2F2*. *hfb_G_000494*, a D1-MSN–specific

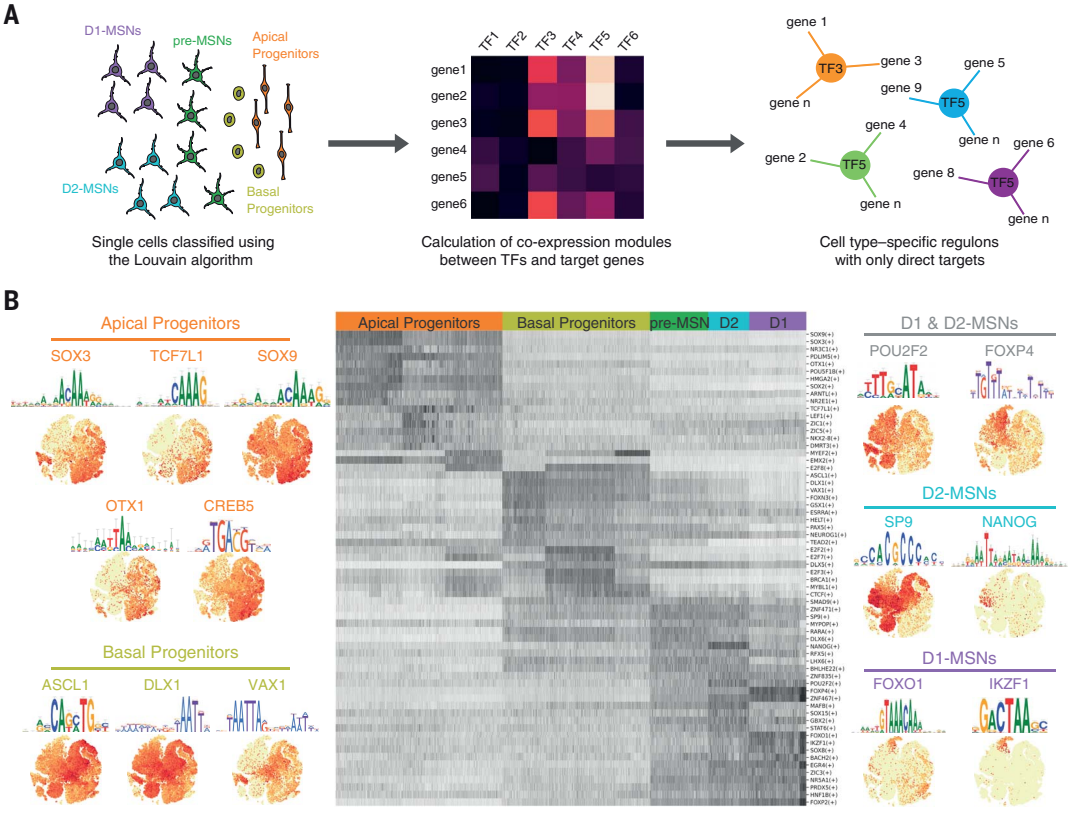

Fig. 3. The cell-specific gene regulatory networks of the LGE lineage. (**A**) Schematic overview of the SCENIC computational approach used to infer cell type–specific gene regulatory networks. (**B**) SCENIC regulon activity matrix showing the top active transcription factors in each cell class. For each cell type, specific transcription factors and their associated motif and expression patterns are shown in t-SNE plots.

lincRNA, shows a connection with *SOX8* and *IKZF1*, two players of the D1-MSN class, whereas many of the D2-MSN–specific lincRNAs are linked to *SP9* and *MAFB*. Overall, these observations reveal insights into how this panel of lincRNAs can be regulated.

LGE and MGE progenitors are transcriptionally distinct

Given the limited information available on APs of the LGE, we then focused our attention on this particular progenitor domain. We found that SOX3 and TCF7L1 (both inhibitors of posteriorizing WNT signals) together with SOX9 (which is induced by SHH signaling) are active TFs that may ventralize and maintain this early progenitor phase (Fig. 4A). Other TFs of this progenitor domain include OTX1, which has been predominantly associated with the CX, and CREB5, which has a role in neural progenitor differentiation. These regulators are interlinked by shared target genes and are likely important for the control of cell fate decisions within the AP domain. The *TCF7L1* network does not share target genes with the other TFs; however, it does regulate genes such as *NKX2.1* and *OTX2* that play a role in maintaining a regional ventral identity (Fig. 4A).

We then investigated whether transcriptional diversity exists at early developmental stages between APs of the LGE and MGE. We combined our set of LGE-specific marker genes (that are not expressed in the CX and MGE) identified in the bulk dataset with the signatures of the different cell states identified in the scRNA-seq dataset (Fig. 4B). We identified 199 genes that are LGE- and cell state–specific (Fig. 4B and table S11); within these, 31 were specific for APs of the LGE, and for two of these candidates—the TF gene *SALL3* and its topologically adjacent *LINC01896* (Fig. 4, C and D)—we confirmed by FISH that they are expressed in APs of the LGE (and CGE) and not in the MGE (Fig. 4E and fig. S10, A to D). Our results propose a model where the neuronal fate of APs in the VZ of the developing striatum is already restricted by a specific topographical and transcriptional program that subsequently drives LGE-specific (versus MGE-specific) cell fates.

Gene network interference reveals key MSN fate determinants

Within the striatum, D1- and D2-MSNs contribute to the direct and indirect pathways, respectively (*15*). We found that both types of MSNs are shaped by a shared set of gene regulatory networks governed by specific MSN "master" TFs (Fig. 5A and fig. S11, A and B). To validate these observations and predict their role in cell lineage determination, we used CellOracle (*16*) to perturb, in silico, these key TFs and their gene regulatory networks. We tested CellOracle on *SP9*, a functionally validated gene in MSN fate determination (*17*). We observed that *SP9* knockout causes a block in BP differentiation, together with a specific arrest in D2-MSN generation, resulting in a shift toward D1-MSN fates (fig. S11C). When we tested *SP9* overexpression, the opposite trend was observed, with a D1- to D2-MSN shift (fig. S11C). This recapitulates what is known about SP9 during striatal development (*17*) and confirms the ability of CellOracle to identify functional TFs. We then tested ZNF467, a zinc finger protein whose function has not yet been characterized in any tissue. We found that its knockout halts MSN differentiation at the progenitor stage, whereas it promotes MSN specification when overexpressed (Fig. 5B). This suggests that ZNF467 may be an important TF for the entire MSN lineage. We then tested *OCT6* and found that knockout of this gene causes an inhibition of the pre-MSN phase, with cells reverting back to progenitor domains and also a stimulation of the transition from pre-MSN to mature MSN states (Fig. 5C). This is in line with the transient nature of *OCT6* expression and may reflect the result of removing this gene at different stages of differentiation. Overexpressing *OCT6* has the opposite effect, as it stalls differentiation in the pre-MSN phase (Fig. 5C). These data confirm the probable function of this gene in the pre-MSN phase, especially in pre-D1 MSNs because we detect OCT6 protein translation mainly in the D1 lineage (Fig. 2, I to L).

We then tested key TFs that may drive the D1-D2 MSN bifurcation point. We found that

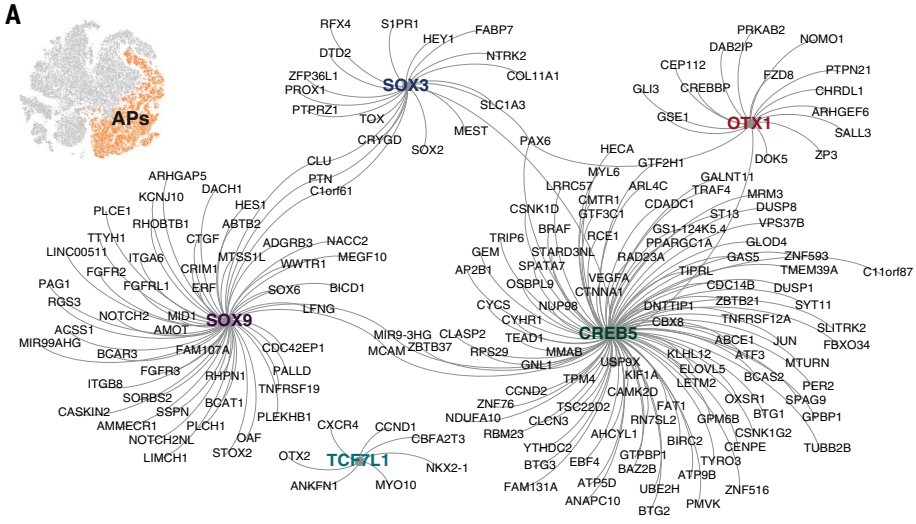

Fig. 4. The emergence of specific apical progenitors within the LGE. (**A**) Specific active regulons in APs. (**B**) Schematic overview of the computational approach used to infer LGE and cell type–specific transcriptional signatures from bulk and scRNA-seq data. DEGs, differentially expressed genes. (**C**) Bulk expression levels of the LGE-specific genes *SALL3* and *LINC01896*. (**D**) Single-cell expression levels (t-SNE plots) of the AP-specific genes *SALL3* and *LINC01896* (*RP11-849I19.1*) in the LGE lineage. (**E**) FISH validation of *SALL3* and *LINC01896* on a telencephalic coronal hemisection at 9 pcw. Upper leftmost panel, DAPI signal. Scale bar, 500 μm. Right panels, probe signals. Scale bar, 200 μm.

IKZF1, an essential gene in the generation of D2-MSNs in mice (*18*), is instead associated to D1-MSNs in humans and therefore may have an opposing role during human development. Perturbation of this gene caused a specific obstruction in D1-MSN maturation, whereas its overexpression led to increased D1 production (Fig. 5D). Finally, we tested MAFB, a specific TF of the D2 lineage that has previously been associated with the survival of MGE-derived cortical interneurons (*19*). Knockout of *MAFB* causes an arrest in BP differentiation and an interruption in D2 production that shifts to the D1 lineage (Fig. 5E), mimicking what is seen with *SP9* knockout. Instead, overexpression of *MAFB* triggers BP maturation and conversion from D1- to D2-MSNs as well as promoting conversion from pre-MSNs to interneurons (Fig. 5E), supporting the role of this gene in promoting this cell class.

Because most studies in humans have generated a general MSN-specific or a D1-MSN–specific signature (*20*), we next decided to characterize a highly specific D2-MSN signature. From our combined bulk and scRNA-seq data (Fig. 4B), we defined 13 specific LGE and D2-MSN genes (table S11). Among them, we validated *LINC01305* and *KCNA5* (fig. S12A), which are specific for the mantle zone (MZ) of the LGE and are not found in the MGE or CGE (fig. S12, B to E).

Finally, to reveal different populations within each major class of MSNs, we performed subclustering of the two classes of MSNs. This revealed two subclusters in both D1- and D2-MSNs (Fig. 5F), and we tested whether these subclusters were already specified in the patch compartment, one of the two major areas (the other being the matrix) that characterize the organization of the striatum, which is formed during early development in mouse models (*21*). A previous single-cell study on postnatal mouse striatal cells (*22*) showed that *Pdyn* and *Tshz1* are specific patch markers. Here, we found that one of the clusters in the D1 population expresses *PDYN* and low levels of *TSHZ1*, whereas in D2-MSNs the opposite trend is observed (Fig. 5F). This suggests that in humans these two markers define MSN lineage–specified patch cells. *PDYN* expression in the MZ confirms that this organization is present at 9 pcw (Fig. 5G). Overall, our data suggest that human MSNs are already compartmentalized in subtype-specific patch regions at this stage of early development.

Human-specific lincRNAs show striatal specificity

We then decided to investigate how lincRNAs define striatal evolution and development. Using liftOver (*23*) and TransMap (*24*), we identified lincRNAs that map across different species, have conserved sequence identity, and are also expressed in the other species considered (Fig. 6A).

Conservation scores showed that lincRNAs identified in the brain exhibit a higher score in primates than in mice, which suggests that they are less conserved in lower mammals (Fig. 6B). However, in all the species considered, conservation scores increased for lincRNAs expressed in the adult brain relative to the developing brain (Fig. 6B). This suggests that the transcriptional complexity of the primate brain, in terms of lincRNAs, is mainly established during fetal development and that in the

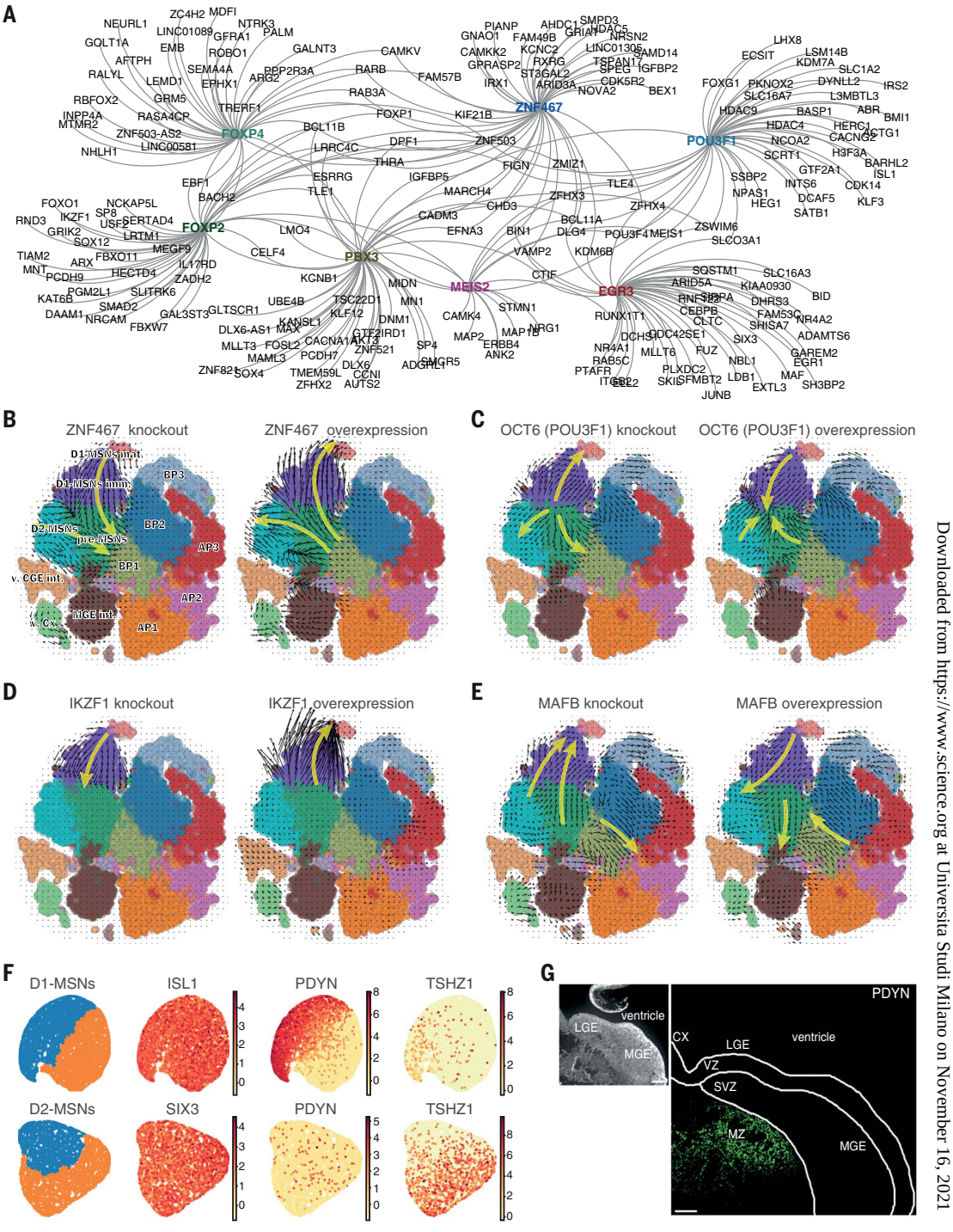

Fig. 5. In silico perturbation of MSN-specific gene regulatory networks. (**A**) Shared active regulons that define D1- and D2-MSNs. (**B** to **E**) CellOracle simulation of knockout and overexpression of the two key MSN markers *ZNF467* (B) and *OCT6* (C); *IKZF1*, a D1-MSN–specific transcription factor (D); and *MAFB*, a D2-MSN–specific transcription factor (E). The effect of the perturbation is shown with projections of cell state transition vectors on each cell's t-SNE plot. Yellow arrows were manually added to represent overall directionality. (**F**) Subclusters of D1- and D2-MSNs, together with expression levels of two specific patch markers (*PDYN* and *TSHZ1*) and canonical D1 (*ISL1*) and D2 (*SIX3*) MSN markers. (**G**) FISH validation of *PDYN* on a telencephalic coronal hemisection shows exclusive expression in the MZ at 9 pcw. Left panel, DAPI signal. Scale bar, 500 μm. Right panel, probe signal. Scale bar, 200 μm.

adult brain this biotype probably possesses more conserved functions among different species.

We further explored two human-specific lincRNAs that were not conserved in the other species considered and that were explicitly expressed in MSNs of the developing human LGE (Fig. 6, C and D). We initially used a guilt-by-association approach (*25*) to investigate the potential function of protein-coding genes that highly correlate with this set of lincRNAs, in order to predict the latter's potential role in MSN specification. We inferred that the MSN-specific lincRNA *hfb_G_000053* could be involved in brain development and neuronal differentiation (Fig. 6E and table S12) and that the mature D1-MSN–specific lincRNA *hfb_G_000494* could function in synaptic organization (Fig. 6F and table S12). When we validated these unannotated lincRNAs by reverse transcription polymerase chain reaction and FISH, we found a specific enrichment of these lincRNAs in the MZ of the developing human striatum relative to the MGE and CGE (Fig. 6, G and H, and fig. S13, A to E).

These findings suggest that these two lincRNAs have a role in the development of human MSNs and may provide insight into how the striatal architecture has evolved to accommodate the expanded human behavioral repertoire.

Discussion

Recent studies of the developing human fetal brain have been crucial in efforts to decipher

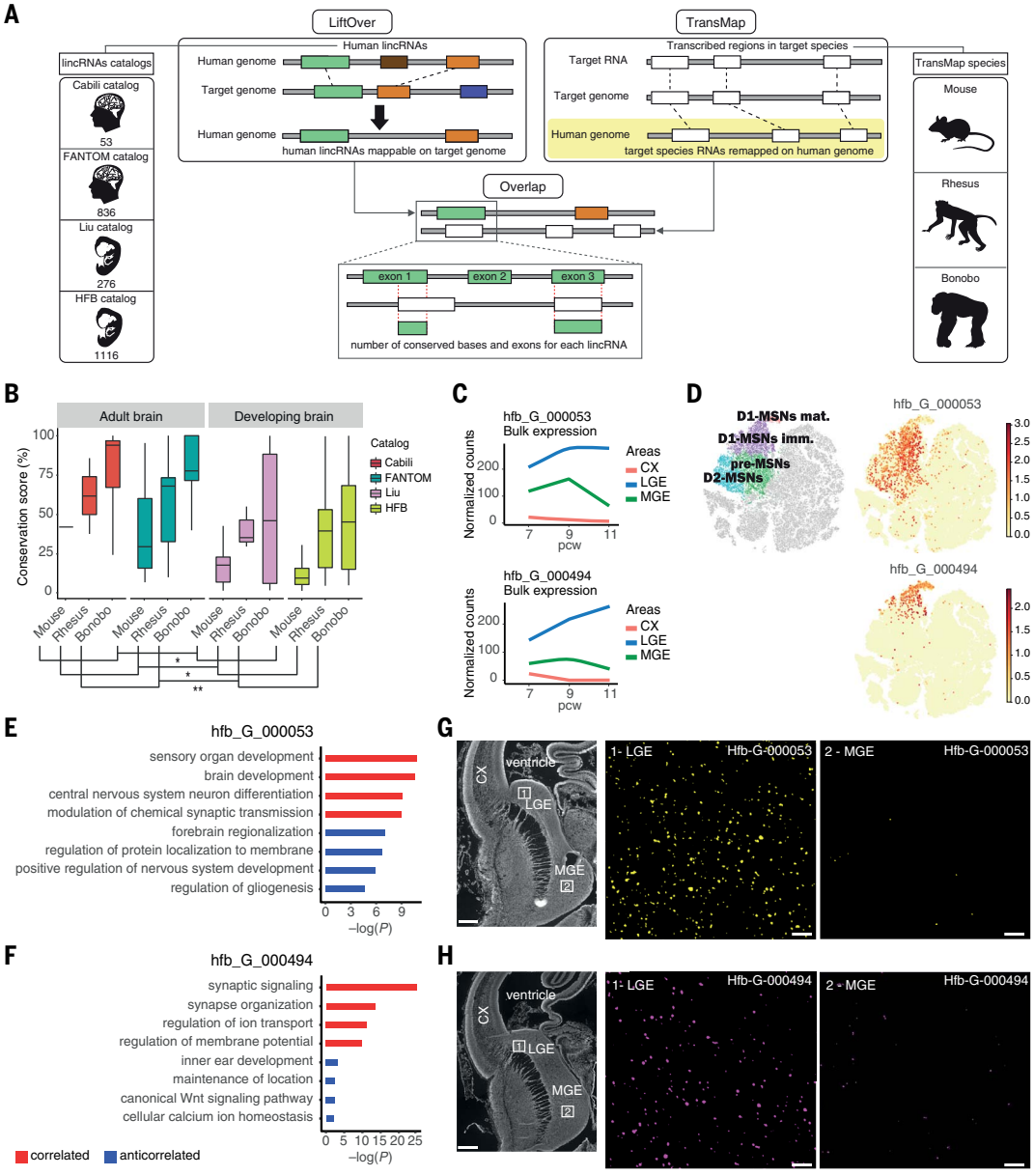

Fig. 6. The human-specific long noncoding signature of MSNs. (**A**) Computational pipeline developed to establish the conservation score of each lincRNA. (**B**) Boxplot showing distribution of conservation scores for different lincRNA classes during development and in adult tissues shows significant differences between lincRNAs identified in the developing brain (Liu, HFB) and those identified in the adult brain (Cabili, FANTOM): *$P < 0.05$, **$P < 0.002$ (Wilcoxon rank-sum test). No differences were observed between the two adult catalogs (Cabili versus FANTOM) or between the two catalogs of the developing brain (Liu versus HFB). (**C**) Bulk expression levels of the human-specific lincRNAs *hfb_G_000053* and *hfb_G_000494*. (**D**) Single-cell expression levels of *hfb_G_000053* and *hfb_G_000494*. (**E** and **F**) Enriched Gene Ontology terms related to genes that have a high correlation or anticorrelation pattern ($P < 0.05$ and $r > 0.6$ or $r < -0.6$) with *hfb_G_000053* (E) and *hfb_G_000494* (F). (**G** and **H**) FISH validation of *hfb_G_000053* (G) and *hfb_G_000494* (H) expression on a telencephalic coronal hemisection at 11 pcw. Leftmost panel, DAPI signal. Scale bar, 500 μm. Right panel, probe signals. Scale bar, 100 μm.

the basis of human brain formation, function, and evolution (*26*–*29*). In this study, we created a high-resolution single-cell map of the early development of the human striatum from a coding and long noncoding perspective. This atlas will pave the way for future integrations with chromatin accessibility data and single-cell proteomics data that will help to resolve the relationship among gene regulation, transcription, and protein production during lineage determination in MSNs, especially at the pre-MSN phase identified in this study.

The main limitation of this work is the high degree of sparsity of the single-cell data. Future protocols with increased sensitivity of RNA detection may reveal new and rare cell types and will probably enable a clearer separation of the pre-MSN phase. This study was also limited by the restricted time window (early fetal development) and brain region (LGE) examined. Studies of both earlier and later developmental time points combined with single-cell measurements of the CX, MGE, and CGE will enhance our understanding of lineage establishment and diversification.

Nonetheless, this study has set the foundation for understanding human striatal development at unprecedented granularity. We foresee that key TFs and lincRNAs defined in this study will be leveraged in vitro to generate authentic MSNs that can serve as suitable donor preparations for future clinical trials in cell replacement therapies. This dataset will also be critical to understand the neurodevelopmental component of Huntington's disease (HD) during striatal development, given the recent evidence of alterations in normal cortical development in human HD fetal samples (*30*). Finally, we also expect that the newly identified human-specific lincRNAs will enable us to understand the underpinnings that characterize human striatum function.

REFERENCES AND NOTES

1. M. A. Raghanti *et al*., Human-specific increase of dopaminergic innervation in a striatal region associated with speech and language: A comparative analysis of the primate basal ganglia. *J. Comp. Neurol.* **524**, 2117–2129 (2016). doi: 10.1002/cne.23937; pmid: 26715195
2. C. R. Gerfen, The neostriatal mosaic: Multiple levels of compartmental organization. *Trends Neurosci.* **15**, 133–139 (1992). doi: 10.1016/0166-2236(92)90355-C; pmid: 1374971
3. S. Grillner, B. Robertson, M. Stephenson-Jones, The evolutionary origin of the vertebrate basal ganglia and its role in action selection. *J. Physiol.* **591**, 5425–5431 (2013). doi: 10.1113/jphysiol.2012.246660; pmid: 23318875

4. J. Stiles, T. L. Jernigan, The basics of brain development. *Neuropsychol. Rev.* **20**, 327–348 (2010). doi: 10.1007/s11065-010-9148-4; pmid: 21042938
5. M. E. Dinger, K. C. Pang, T. R. Mercer, J. S. Mattick, Differentiating protein-coding and noncoding RNA: Challenges and ambiguities. *PLOS Comput. Biol.* **4**, e1000176 (2008). doi: 10.1371/journal.pcbi.1000176; pmid: 19043537
6. S. Djebali *et al*., Landscape of transcription in human cells. *Nature* **489**, 101–108 (2012). doi: 10.1038/nature11233; pmid: 22955620
7. M. N. Cabili *et al*., Integrative annotation of human large intergenic noncoding RNAs reveals global properties and specific subclasses. *Genes Dev.* **25**, 1915–1927 (2011). doi: 10.1101/gad.17446611; pmid: 21890647
8. C. C. Hon *et al*., An atlas of human long non-coding RNAs with accurate 5′ ends. *Nature* **543**, 199–204 (2017). doi: 10.1038/nature21374; pmid: 28241135
9. S. J. Liu *et al*., Single-cell analysis of long non-coding RNAs in the developing human neocortex. *Genome Biol.* **17**, 67 (2016). doi: 10.1186/s13059-016-0932-1; pmid: 27081004
10. G. La Manno *et al*., RNA velocity of single cells. *Nature* **560**, 494–498 (2018). doi: 10.1038/s41586-018-0414-6; pmid: 30089906
11. V. Bergen, M. Lange, S. Peidli, F. A. Wolf, F. J. Theis, Generalizing RNA velocity to transient cell states through dynamical modeling. *Nat. Biotechnol.* **38**, 1408–1414 (2020). doi: 10.1038/s41587-020-0591-3; pmid: 32747759
12. M. Melé *et al*., Chromatin environment, transcriptional regulation, and splicing distinguish lincRNAs and mRNAs. *Genome Res.* **27**, 27–37 (2017). doi: 10.1101/gr.214205.116; pmid: 27927715
13. J. Q. Wu *et al*., Dynamic transcriptomes during neural differentiation of human embryonic stem cells revealed by short, long, and paired-end sequencing. *Proc. Natl. Acad. Sci. U.S.A.* **107**, 5254–5259 (2010). doi: 10.1073/pnas.0914114107; pmid: 20194744
14. S. Aibar *et al*., SCENIC: Single-cell regulatory network inference and clustering. *Nat. Methods* **14**, 1083–1086 (2017). doi: 10.1038/nmeth.4463; pmid: 28991892
15. D. J. Surmeier, W. J. Song, Z. Yan, Coordinated expression of dopamine receptors in neostriatal medium spiny neurons. *J. Neurosci.* **16**, 6579–6591 (1996). doi: 10.1523/JNEUROSCI.16-20-06579.1996; pmid: 8815934
16. K. Kamimoto, C. M. Hoffmann, S. A. Morris, CellOracle: Dissecting cell identity via network inference and in silico gene perturbation. bioRxiv [preprint]. 17 February 2020. pmid: 947416
17. Q. Zhang *et al*., The Zinc Finger Transcription Factor Sp9 Is Required for the Development of Striatopallidal Projection Neurons. *Cell Rep.* **16**, 1431–1444 (2016). doi: 10.1016/j.celrep.2016.06.090; pmid: 27452460
18. R. Martín-Ibáñez *et al*., Ikaros-1 couples cell cycle arrest of late striatal precursors with neurogenesis of enkephalinergic neurons. *J. Comp. Neurol.* **518**, 329–351 (2010). doi: 10.1002/cne.22215; pmid: 19950118
19. E. L. L. Pai *et al*., *Maf* and *Mafb* control mouse pallial interneuron fate and maturation through neuropsychiatric disease gene regulation. *eLife* **9**, e54903 (2020). doi: 10.7554/eLife.54903; pmid: 32452758
20. M. Onorati *et al*., Molecular and functional definition of the developing human striatum. *Nat. Neurosci.* **17**, 1804–1815 (2014). doi: 10.1038/nn.3860; pmid: 25383901
21. S. M. Kelly *et al*., Radial Glial Lineage Progression and Differential Intermediate Progenitor Amplification Underlie Striatal Compartments and Circuit Organization. *Neuron* **99**, 345–361.e4 (2018). doi: 10.1016/j.neuron.2018.06.021; pmid: 30017396
22. A. Saunders *et al*., Molecular Diversity and Specializations among the Cells of the Adult Mouse Brain. *Cell* **174**, 1015–1030.e16 (2018). doi: 10.1016/j.cell.2018.07.028; pmid: 30096299
23. R. M. Kuhn, D. Haussler, W. J. Kent, The UCSC genome browser and associated tools. *Brief. Bioinform.* **14**, 144–161 (2013). doi: 10.1093/bib/bbs038; pmid: 22908213
24. J. Zhu *et al*., Comparative genomics search for losses of long-established genes on the human lineage. *PLOS Comput. Biol.* **3**, e247 (2007). doi: 10.1371/journal.pcbi.0030247; pmid: 18085818
25. M. Guttman *et al*., Chromatin signature reveals over a thousand highly conserved large non-coding RNAs in mammals. *Nature* **458**, 223–227 (2009). doi: 10.1038/nature07672; pmid: 19182780
26. T. J. Nowakowski *et al*., Spatiotemporal gene expression trajectories reveal developmental hierarchies of the human cortex. *Science* **358**, 1318–1323 (2017). doi: 10.1093/bib/bbs038; pmid: 22908213
27. G. La Manno *et al*., Molecular Diversity of Midbrain Development in Mouse, Human, and Stem Cells. *Cell* **167**, 566–580.e19 (2016). doi: 10.1016/j.cell.2016.09.027; pmid: 27716510
28. X. Fan *et al*., Single-cell transcriptome analysis reveals cell lineage specification in temporal-spatial patterns in human cortical development. *Sci. Adv.* **6**, eaaz2978 (2020). doi: 10.1126/sciadv.aaz2978; pmid: 32923614
29. S. Zhong *et al*., A single-cell RNA-seq survey of the developmental landscape of the human prefrontal cortex. *Nature* **555**, 524–528 (2018). doi: 10.1038/nature25980; pmid: 29539641
30. M. Barnat *et al*., Huntington's disease alters human neurodevelopment. *Science* **369**, 787–793 (2020). doi: 10.1093/bib/bbs038; pmid: 22908213

ACKNOWLEDGMENTS

We thank C. Cordiglieri and A. Fasciani of the INGM Imaging Facility (Istituto Nazionale Genetica Molecolare–INGM, Milan, Italy) for scientific and technical assistance, and S. Noble of the CHDI Foundation for help with manuscript editing. **Funding:** This work was conducted with collaboration and funding from CHDI Foundation (JSC A11103), a nonprofit biomedical research organization exclusively dedicated to developing therapeutics that will substantially improve the life of individuals affected by HD, to E.C. This study was also supported by the European Union–funded projects NeurostemcellRepair (FP7, GA no. 602278, 2013-17) and NSC-Reconstruct (H2020, GA no. 874758, 2020-23) to E.C. and R.A.B. The fetal tissue collection in Cambridge is supported by NIHR funding of the Biomedical Research Centre and by the Wellcome Trust 203151/Z/16/Z. **Author contributions:** V.D.B. and E.C. conceived the study; V.D.B., P.C., E.V., D.B., and E.C. designed the experiments; V.D.B. performed computational analysis with contributions from C.C., T.L., V.R., R.J.P.B., F.G., and M.P.; C.C., V.D.B., and G.P. performed the conservation analysis study; P.C. performed the bulk and single-cell experiments with contributions from D.B., I.E.-C., A.F., M.D.S., and G.R.; E.V. performed FISH analysis; M.G. performed immunohistochemistry analysis; V.R., R.J.P.B., F.G., M.D.S., G.R., and M.P. contributed the INGM single-cell and bioinformatics platforms; X.H., R.V., and R.A.B. collected the fetal samples and performed the dissection; K.K. and S.A.M. performed in silico perturbation analysis with V.D.B. and R.J.P.B.; J.C., D.F., M.P., and E.C. contributed to data elaboration and presentation. All authors contributed to interpretation of the results. Figures were assembled by V.D.B. together with T.L. The manuscript was written by V.D.B., revised by D.B. and E.C., and edited and proofread by all authors. E.C. proposed the research program, secured the funding, established the collaborations, and coordinated the study. **Competing interests:** The authors declare no competing interests. **Data and materials availability:** All bulk and scRNA-seq data have been deposited in the ArrayExpress database at EMBL-EBI (www.ebi.ac.uk/arrayexpress/) under accession no. E-MTAB-8893 (bulk RNA-seq) and E-MTAB-8894 (scRNA-seq). All other data are present in the main paper or the supplement.

SUPPLEMENTARY MATERIALS

science.sciencemag.org/content/372/6542/eabf5759/suppl/DC1
Materials and Methods
Figs. S1 to S13
Tables S1 to S12
References (*31*–*48*)

4 November 2020; accepted 29 March 2021
10.1126/science.abf5759

Science

The coding and long noncoding single-cell atlas of the developing human fetal striatum

Vittoria Dickinson BocchiPaola ConfortiElena VezzoliDario BesussoClaudio CappadonaTiziana LischettiMaura GalimbertiValeria RanzaniRaoul J. P. BonnalMarco De SimoneGrazisa RossettiXiaoling HeKenji KamimotoIra Espuny-CamachoAndrea FaedoFederica GervasoniRomina VuonoSamantha A. MorrisJian ChenDan FelsenfeldGiulio PavesiRoger A. BarkerMassimiliano PaganiElena Cattaneo

Science, 372 (6542), eabf5759. • DOI: 10.1126/science.abf5759

Development of the human striatum revealed

Deep in the brain, the striatum receives and coordinates inputs from other parts of the brain. Bocchi *et al.* surveyed molecular features as the striatum develops in the human brain. Single-cell surveys of long intergenic noncoding RNAs revealed a progenitor for medium spiny neurons and provide insight into evolutionary divergence of this critical part of the brain.

Science, this issue p. eabf5759

Science (ISSN 1095-9203) is published by the American Association for the Advancement of Science. 1200 New York Avenue NW, Washington, DC 20005. The title *Science* is a registered trademark of AAAS.